JoTSE (2010) ISSN: 1949-4866
Volume 1, Issue 1/2, pp.

ON THE DEFORMATION OF A HARD COATING/SOFT SUBSTRATE SYSTEM UNDER SPHERICAL NANOINDENTATION: A BOUNDARY ELEMENT NUMERICAL ANALYSIS

N. Oumarou*[a], R. Kouitat Njiwa [a], Ph. Stempflé [b] and J. von Stebut [a]

[a]Institut Jean Lamour – MMNPS – Département SIMM – CNRS (UMR 7198) – INPL – Nancy Université, Ecole des Mines, Parc de Saurupt, CS14234, 54042 Nancy Cedex, France

[b]Institut FEMTO-ST (UMR CNRS 6174 – Université de Franche Comté – CNRS – ENSMM – UTBM), ENSMM, 26 Chemin de l'Epitaphe, F-25030 Besançon Cedex, France

ABSTRACT

We present the boundary element numerical analysis of spherical depth sensing indentation. The study aims to pinpoint some aspects of the deformation process thus highlighting simple and sufficiently accurate relations allowing a rapid analysis of experimental data. Results mainly concern elastic deformation of hard thin film coatings on an elastic-plastic substrate.

First a well known and useful relation between the penetration and the projected contact area in the case of the elastic indentation of an isotropic homogeneous half space is shown to remain valid in the elastic-plastic deformation regime as well as in the case of a thin film/substrate system. It is also shown that the radius of the pile-up forming during unloading on the residual imprint is (approximately three times) larger than the contact radius at maximum load. Finally a careful analysis of the stress field evolution during the deformation process is presented.

Keywords: Indentation, Elastoplastic strain, von Mises Stress, Film–substrate system, Young's modulus, Hardness.

* Corresponding author, oumarou@mines.inpl-nancy.fr

LIST OF NOTATIONS

E:	Young's modulus
E^f:	film Young's modulus
E^i:	indenter Young's modulus
E^S:	substrate Young's modulus
ν:	Poisson's ratios
ν^f:	film Poisson's ratio
ν^i:	indenter Poisson's ratio
ν^S:	substrate Poisson's ratio
σ_y:	yield stress
σ_y^S:	substrate yield stress
R:	indenter radius
t^f:	film thickness
r:	radial coordinate
Z:	axial coordinate
ε^p:	plastic strain tensor
σ^p	plastic stress tensor
F:	maximal applied load
F^*:	applied load of first material yielding
h:	indenter maximal displacement
a:	contact radius at maximal load
a^*:	contact radius at first yielding
δ:	relative approach
P_m:	mean pressure
σ_r^Z:	axial residual stress
σ_{vM}:	von Mises equivalent Stress
r_p:	radius of plastic zone
z_p:	depth of plastic zone

1. INTRODUCTION

Depth sensing indentation, often called nano-indentation, is increasingly retained for the assessment of mechanical characteristics of various types of media, for which common homogeneous mechanical tests cannot be performed or are extremely difficult to perform. This is particularly true for coating/substrate systems engineered for contact mechanical applications for which the coating generally has high hardness – *i.e.* a high tensile yield stress. The use of depth sensing indentation also enables simulation of the single asperity contact problem which is of paramount importance for the understanding and modelling of tribological processes such as friction and wear (e.g. Bhushan, 1999; and references therein). When analysing monolithic homogeneous materials the continuously recorded load *vs*. indenter displacement plot enables an assessment of mechanical properties such as Young's modulus (E), hardening exponent (n) and yield stress (σ_y). The contact area between the

punch and the specimen is of paramount importance for the analysis of the experiment. It is commonly determined indirectly following the methodologies proposed by Oliver and Pharr, 1992; and, in the specific case of spherical indenter, by Field and Swain, 1993. The Oliver-Pharr method is based on an elastic contact recovery which avoids the use of the experimentally assesse residual imprint geometry. The method exclusively uses the initial part of the unloading indentation curve where it is assumed that the onset of material recovery has an elastic behaviour. Even in the case of well performed experiments, the corresponding material parameters may deviate from those provided by other methods such as the tensile test.

According to some authors piling-up and sinking-in phenomena around the residual imprint could be an explanation. A lot of research has been done on the influence of these phenomena on the indentation results (e.g. Garrido and Rodriguez, 2005; Bolshakov and Pharr 1998). Also suggestions to account for these phenomena have been proposed as the replacement of the contact area in the Oliver and Pharr method by the one obtained from post-test SEM pictures (e.g. McElhaney et al, 1998) or from AFM topography (e.g. Saha and Nix, 2001; 2002; Stempflé and von Stebut, 2006). By doing so, it is generally assumed that piling-up occurs during loading and will affect the contact area at maximum load. Using finite element modelling, some authors have investigated the formation of piling-up and sinking-in with respect to the mechanical properties of the material (e.g. Taljat and Pharr, 2004; Mesarovic and Fleck, 1999; Mata et al, 2002).

It appears that these phenomena are controlled by the non-dimensional parameters E/σ_y and n where E is the Young modulus, σ_y the yield stress and n hardening exponent. To our knowledge, such studies are not concerned with the case of film-substrate systems. In this case, most of the work focuses on the state of stress beneath the indenter. When looking for material properties of such systems, the Oliver-Pharr method originally designed for isotropic homogeneous materials is still adopted. The composite material parameters obtained at different loads are modelled by an empirical law which is extrapolated to zero penetration in order to deduce film properties and to high penetration for substrate material parameters. Some usually neglected effects are the sensitivity to indentation size effect at low loads (Fischer-Cripps, 2002) and to the substrate effect at high loads (Saha and Nix, 2002; Kouitat and von Stebut, 2003).

In the present work we check and substantiate some commonly accepted experimental assertions regarding depth sensing indentation of a hard coating on a softer substrate. The main steps of the specifically developed numerical tool based on the field boundary element method are briefly recalled in section 2. In section 3, for low indentation loads, the validity of the link between the relative approach and the projected contact area is analysed. It is shown that the elastic film increases the radius of the residual imprint when measured at the summit of the pile-up. It is also shown that unloading may be accompanied by plastic flow leading to high tensile stresses at the interface between the film and the substrate.

2. METHOD OF SOLUTION

Let Γ be the boundary of Ω the geometrical domain filled by the material of the solid (figure 1).

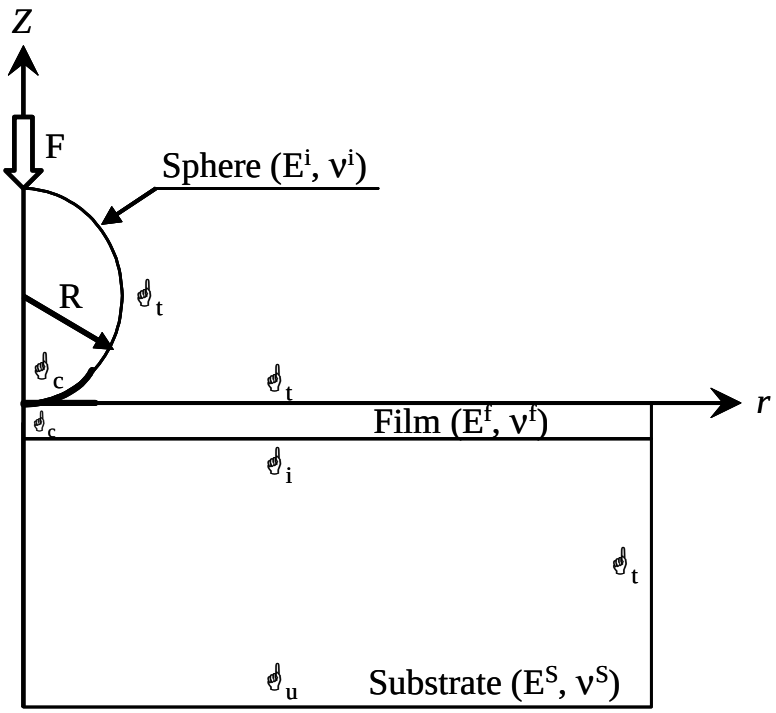

Figure 1. A sphere with radius R is indenting an elastic film with thickness t^f bonded onto an elasto-plastic substrate.

Consider the solution of an elastic-plastic problem under the small strain assumption, using cylindrical coordinates, the necessary boundary integrals are:

- the displacement boundary integral equation:

$$u_j(y)\int_\Gamma D_{ij}(x,y)d\Gamma(x)+\int_\Gamma T_{ij}(x,y)(u_j(x)-u_j(y))r\,d\Gamma(x)= \int_\Gamma U_{ij}(x,y)t_j(x)r\,d\Gamma(x)+\int_{\Omega_p} U_{ia,b}(x,y)\sigma^p_{ab}(x)r\,d\Omega(x) \quad (1)$$

where i, j = r, z; a, b = r, z, θ and differentiation represented by a comma is a cylindrical one (see Kuhn et *al*, 1998). $\sigma^p_{ij}(x)= C_{ijkl}\varepsilon^p_{kl}(x)$ (i, j = r, θ, z) is the plastic stress tensor and C_{ijkl} the usual elasticity tensor. The singular influence functions appearing in the above integral can be found in the literature (e.g. Balas et al., 1989; Henry and Banerjee, 1988).

- the displacement gradient boundary integral equation:

Let *y* be a point not located on the boundary Γ. The displacement gradient at y is obtained by differentiation of (1):

$$\frac{\partial u_i}{\partial y_l}(y)=\int_\Gamma [\frac{\partial U_{ij}}{\partial y_l}(x,y)t_j(x)-\frac{\partial T_{ij}}{\partial y_l}(x,y)u_j(x)]r\,d\Gamma(x) + \frac{\partial}{\partial y_l}\int_{\Omega_p} U_{ia,b}(x,y)\sigma_{ab}^p(x)\,r\,d\Omega(x) \quad (2)$$

Because of the domain integrals in relations (1) and (2), volume cells are required when implementing the method. Since they are limited to that part of the body where plastic flow is expected, the method is particularly attractive for the simulation of indentation problems (limited plastic volume compared to specimen size).

As usual, equations (1) and (2) are discretized and systems of equations are obtained with unknowns as boundary displacement and traction and plastic stress. Though the solution can be obtained by the variable stiffness approach (Henry and Banerjee, 1988), we have adopted the radial return algorithm (Bonnet and Mukherjee, 1996) which is an implicit strategy based on the concept of consistent tangent operator. As for the unilateral contact boundary condition the min function reformulation is adopted and the resulting non-differentiable system of equations is solved following the strategy proposed in the context of the finite element method by Christensen et al, 1998.

3. RESULTS AND DISCUSSION

3.1. Indentation of a Homogeneous Elastic-Plastic Specimen

Let us first, consider a homogeneous flat with known mechanical parameters (Young's modulus, Poisson ratio and yield stress). Spherical indentation of elastic-plastic materials has been extensively studied by a number of workers, and is considered herein mainly to validate the specifically built numerical tool and emphasize some basic results of ball on flat depth sensing indentation.

Given an elastically deformable punch with radius R (Young's modulus E^i and Poisson ratio ν^i), the load for the onset of plastic flow as well as the location of the first yield point within the sample are known from Hertzian theory of contact. These values resulting from our numerical tool are in excellent agreement with theoretical prediction.

In the plastic regime, agreement is observed with results reported by Edlinger et al., 1993; in the case of the large indenter radius (500mm) and by Hardy et al., 1971; also presented in the book by K.L. Johnson, 1985. In particular, let us point out the presence of an elastically strained zone just below the contact area (cf. Figure 2).

This region, situated just above the first yielding point within the specimen remains unchanged during the entire deformation process. This means that the yield zone first expands laterally and downwards. Then there is an upwards expansion through the free surface which is followed by the fully plastic regime. Compared to other commonly adopted indenter geometries, this is another distinctive feature of spherical indentation.

Regarding the loading/unloading curve, numerical experiments on specimens with various mechanical properties have been carried out. In the considered range of deformation,

it is observed that even within plastic regime, the product of the relative approach of the two bodies in contact, δ, and the radius of curvature of the punch, R, equals the square of the projected contact area as given by Hertzian theory of elastic contact, i.e., $\delta = \frac{a^2}{R}$.

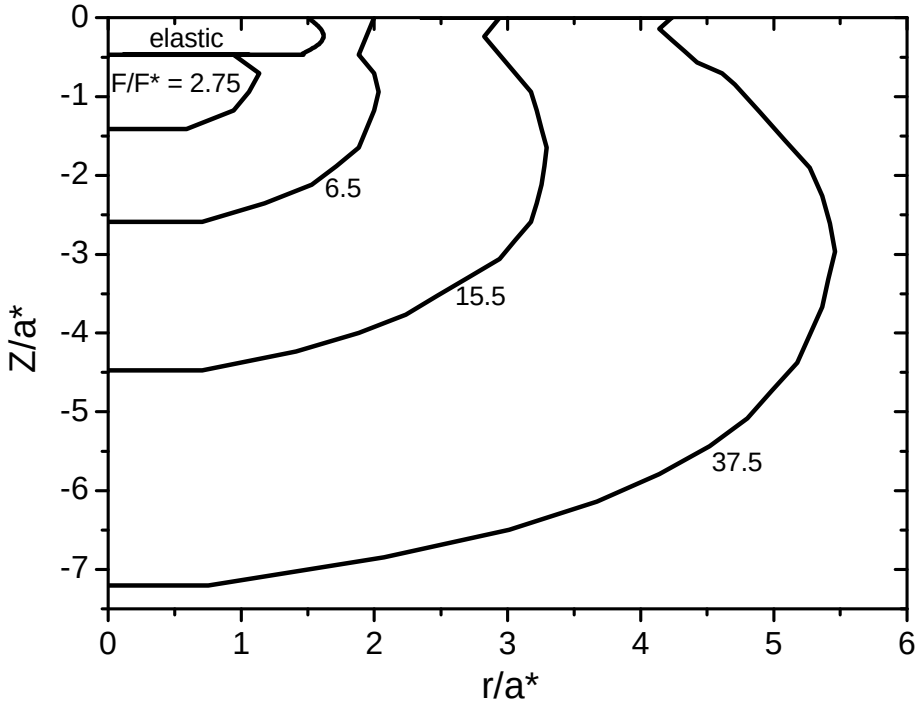

Figure 2. Evolution of the plastic contour in the homogenous medium with the load level applied; *a** is the radius contact corresponding of the load F* of initiation of plasticity in the homogeneous medium.

Let us recall that in the limiting case of a rigid punch the relative approach equals the punch displacement. According to this result, depth-sensing indentation data can be represented in terms of the mean pressure vs. indentation strain (*a*/R*)* as shown in Figure 3. When free from experimental artefacts related to "contact establishment" the *initial part of the loading curve* is linear and the slope of the approximating line can be used to assess the indentation elastic modulus of the material. Indeed, it follows the Hertzian straight line of the problem. This is an alternative to the popular Oliver - Pharr methodology for the determination of the Young's modulus and the hardness (mean pressure). It should be mentioned that the use of the indentation loading curve for such a purpose has already been proposed by Loubet et al., 1986 for the Vickers geometry.

Let us now investigate how these simple results are modified when a thin hard film is present at the specimen surface.

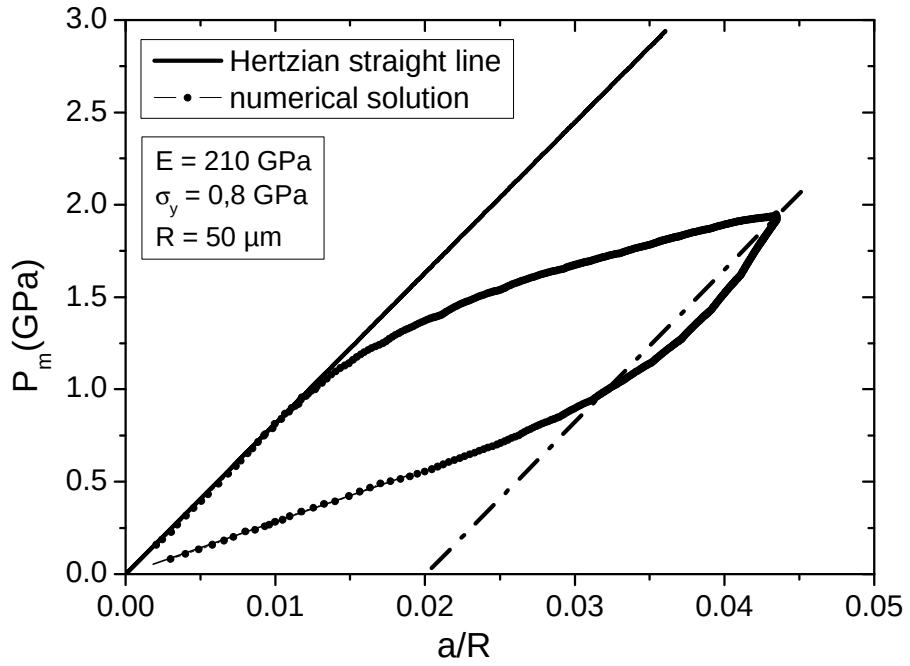

Figure 3. Homogenous medium (E = 210 GPa, σ_y = 0.8 GPa, R = 50 µm). Load/unload plots of the mean pressure vs. indentation strain. Solid line: elastic mean pressure. Dashed line: parallel of the mean pressure line passing through the first unloading point. (Load of initiation of plasticity in the homogeneous medium: F* = 0.8 mN).

3.2. Indentation of a Hard Coating/Softer Substrate System

For the remainder of the analysis, we adopt the following conditions. Young's modulus and the Poisson ratio of the 50 µm radius spherically tipped diamond indenter are 1140 GPa and 0.07 respectively. The substrate is considered as an elastic perfectly plastic stainless steel with Young's modulus E^s = 210 GPa, Poisson ratio ν^s = 0.3 and yield stress σ_Y^s = 0.8 GPa. Its dimensions are chosen such that it can be considered as a half space. The hard film with thickness 3 µm, Young's modulus $E^f = 2E^s$ = 420 GPa, and a Poisson ratio ν^f = 0.3, is assumed to deform only elastically within the loading range. The indentation depth remains less than 10% of the film thickness for all the maximum, loads applied.

3.2.1. Load / Unload Resulting Surface Characteristics and Topography

The useful relation $\delta = \frac{a^2}{R}$ has already been demonstrated to remain valid in the case of elastic spherical indentation of a film/substrate specimen by Kouitat and von Stebut, 2003. Surprisingly, despite the plastic deformation of the substrate, numerical results show that this relation is valid upon loading as well as unloading. Therefore, in this case also, the result of depth sensing indentation can be represented in terms of mean pressure versus indentation

strain as shown in figure 4. Here again, the first part of the loading plot is linear with a slope related to a material parameter. Our investigations reveal that it is related to Young's modulus of the film only (cf. figure 4). The initial part of the unloading curve is also linear, but now with a slope related to a composite Young's modulus instead (cf. figure 4). Hence, it is possible to extract the film Young's modulus from spherical depth sensing indentation experiment.

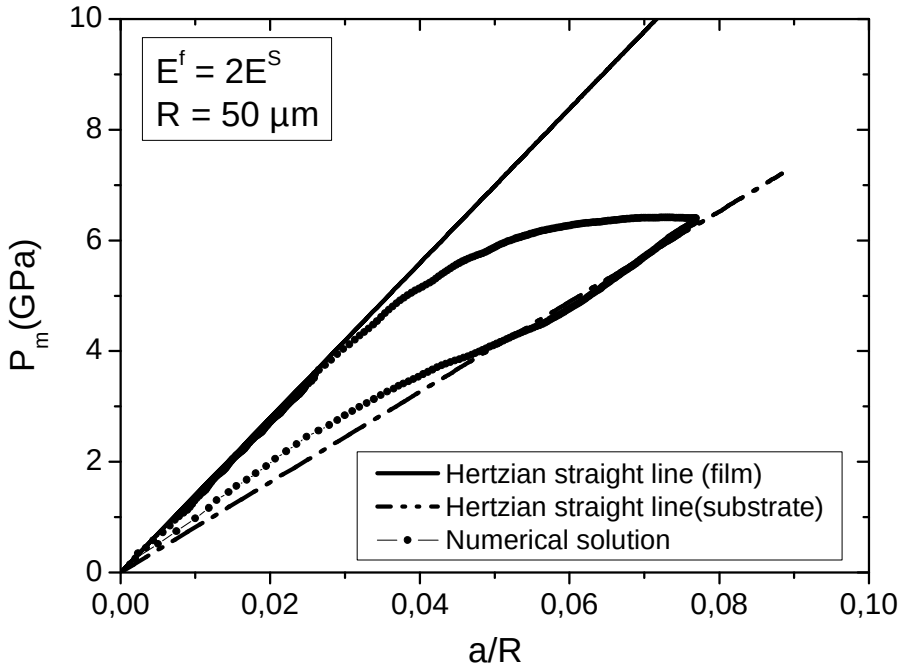

Figure 4. Film/substrate system (E^S = 210 GPa, σ_y^S = 0.8 GPa, E^f/E^S = 2, t^f = 3 µm, R = 50 µm). Load/unload plots of the mean pressure vs. indentation strain. Solid line: elastic mean pressure with film material properties. Dashed line: elastic mean pressure with substrate material properties.

Let us now consider the residual profile of the indent. Denote by F* the load at first yielding in the substrate as obtained from simulation. Figures 5a and 5b show the residual indent profile at the free surface and at the interface respectively for different values of the maximum load F.

Within computational precision the lateral pile-up amplitude is identical in both cases. As for indentation of the homogeneous substrate alone, relative elastic recovery decreases with increasing load. For the coated specimen this holds both at the interface and at the free surface. However, the residual depth is slightly more important at the interface than at the free surface. As a consequence, a tensile stress along the axis normal to the specimen surface must be present in the surface volume below the contact area. Let us point out that in all cases retained in the present study, piling up that can only be observed experimentally after completion of a closed cycle and is shown numerically to occur essentially during unloading.

An additional striking feature is the position of the pile-up apex, which for the coated specimen, is way beyond that of the contact radius *a* at preceding maximum load - i.e. at roughly 3.5*a* while it was 1.2*a* for the uncoated substrate material.

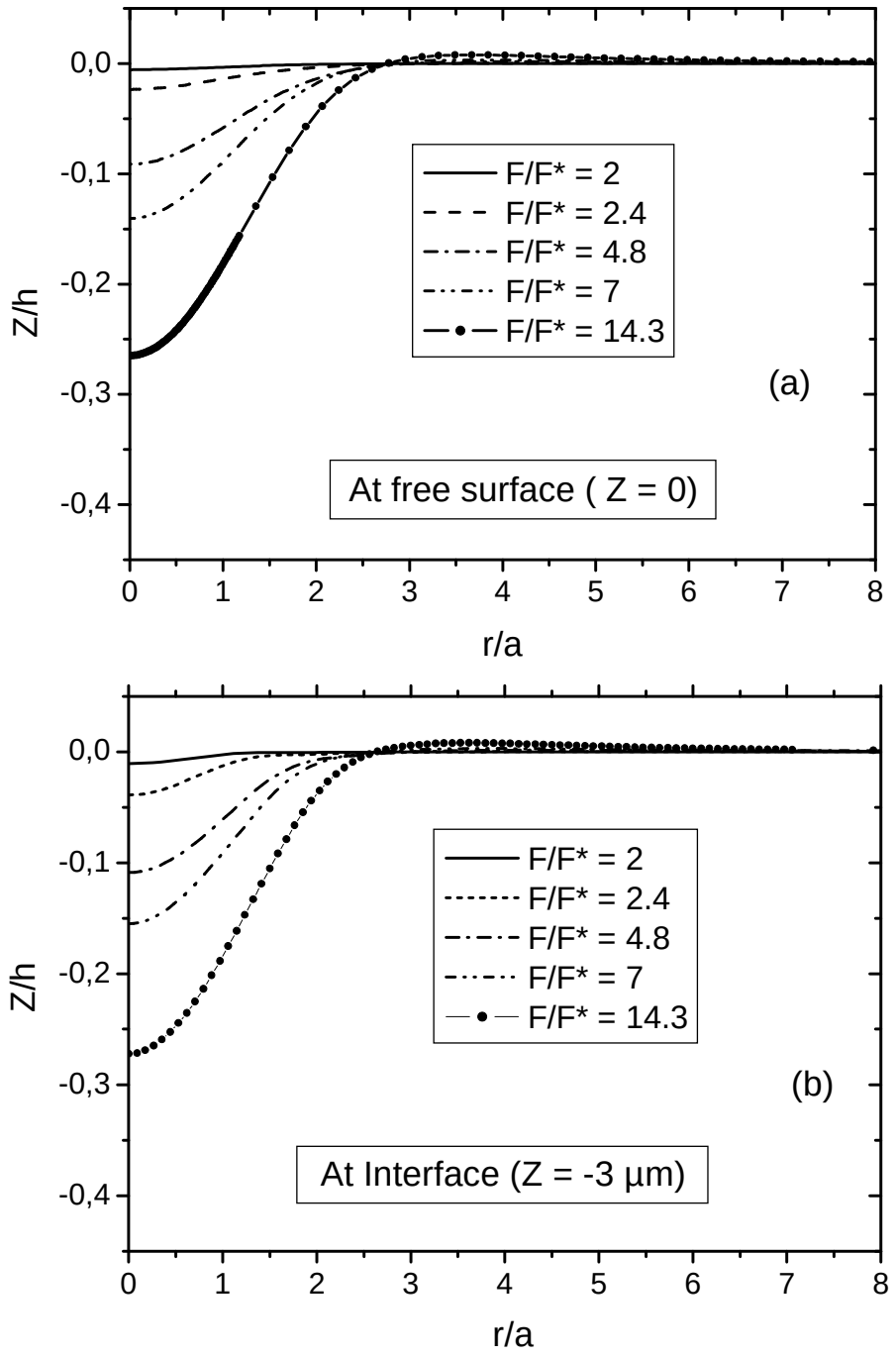

Figure 5. Film/substrate system (R = 50 µm, $E^f/E^S = 2$, $t^f = 3$ µm); Profile of the residual indent for different maximum load levels F < 300 m (*a* is the contact radius at maximum load); a) at the free surface and b) at the interface.

This result implies that for the contact geometry considered (R = 50 µm, t^f = 3 µm), whatever the adopted approach, experimental determination of the real contact area based on the observable diameter of the residual plastic indent is considerably higher than that computed at maximum contact load.

3.2.2. Stress Fields

a) Stress Fields in Substrate at Maximum Load

For convenience the stress values have been normalized with respect to the stress of first yielding in the substrate. Figure 6 shows the subsurface stress field in the substrate for a maximum contact load F = 100 mN (F/F* = 4.8). According to figure 5b, this corresponds to a residual indent depth less than $1/10^{th}$ the coating thickness. It follows from figure 6 that a zone of plasticised material is situated in the substrate right below the interface.

Some remarks are worthwhile concerning the dimension of the contact radius *a* at maximum applied load during the indentation and the maximum half width (r_p) of the plastically deformed substrate volume. For the loading conditions considered r_p is situated at the interface and extends to roughly 5 µm. This is twice that of *a*, which substantiates the above finding about the position of the pile-up apex. If z_p is the maximum depth of the plastic zone below the interface we find $r_p > z_p$.

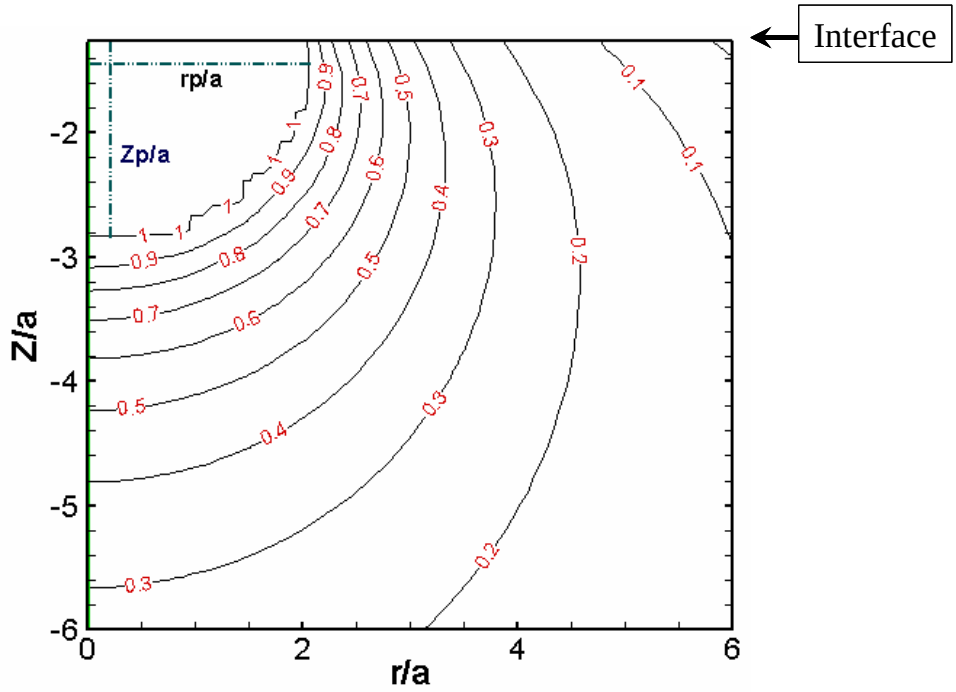

Figure 6. Film/substrate system (R = 50 µm, E^f/E^S = 2, t^f = 3 µm); F = 100 mN (F/F* = 4.8); Contour plot of the normalised von Mises stress σ_{vM}/σ_y^S; case of *rp* greater than z*p*. The contact radius at this load level is *a* = 2.4 µm (interface: *Z/a* = - 1.26).

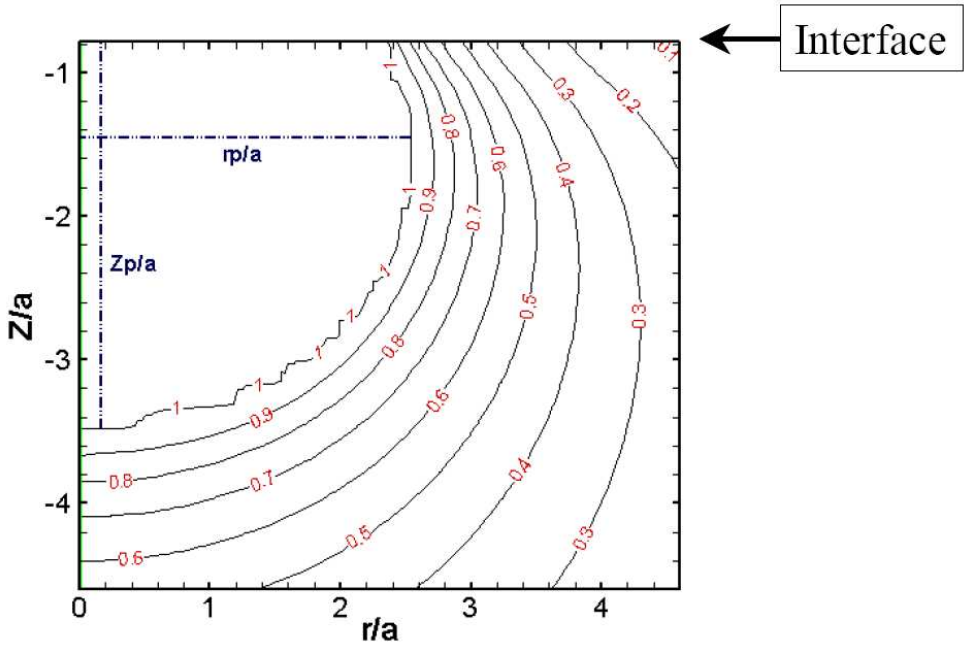

Figure 7. Film/substrate system (R = 50 µm, E^f/E^S = 2, t^f = 3 µm); F = 300 mN (F/F* = 14.3); Contour plot of the von Mises stress; Case with *rp* less than *zp*; The contact radius at this level load is *a* = 3.8 µm (interface: *Z*/*a* = - 0.79).

Figure 7 is analogous to Figure 6 except for considerably higher contact loads leading to a substantially larger plastically deformed volume in the substrate. In this case, the maximum half width has shifted into the depth of the substrate and now $r_p < z_p$ with r_p/a = 2.6.

From the r_p/a ratio, it is confirmed that the above numerical results concerning the apparent contact radii generated with fairly blunt (50 µm radius) indenters after complete unloading are related to the presence of a plastic zone spreading laterally within the substrate well beyond the corresponding contact radii at maximum applied load.

In conclusion, when increasing the contact load, when the Hertzian point (*a*/2) is located within the film, plastic yielding starts in the substrate just below the interface and the plastic volume first expands more rapidly along the interface than into depth. For contact loads well beyond initial yielding this situation is inverted.

b) Stress Fields during Unloading

In depth sensing indentation the first part of the unloading plot is commonly used to determine the contact stiffness and the resulting elastic modulus (Oliver and Pharr, 1992). This implies that, alike unloading in tensile testing; the deformation process is elastic.

The validity of this assumption is checked numerically for the entire unloading phase of an indentation experiment. In figures 8a-f, the von Mises stress field, σ_{vM}, is shown after 10, 20, 30, 40, 50 and 100% unloading from the situation of figure 7.

At 10% unloading (figure 8a), the contour lines of σ_{vM}/σ_y^s indicate an entirely elastic process within the specimen. However, it should be noted that the stress decreases more rapidly in the formerly plasticized substrate zone.

This tendency prevails up to 30% unloading (figure 8c) where a point of zero stress appears on the axis of symmetry. At 40% unloading (figure 8d) this point has transformed into an elliptical contour line with one end on the axis of symmetry and the other just below the interface. Within this elliptical region stresses are higher than in the preceding unloading level. At subsequent unloading, the axis of the ellipse increases and its centre moves downwards.

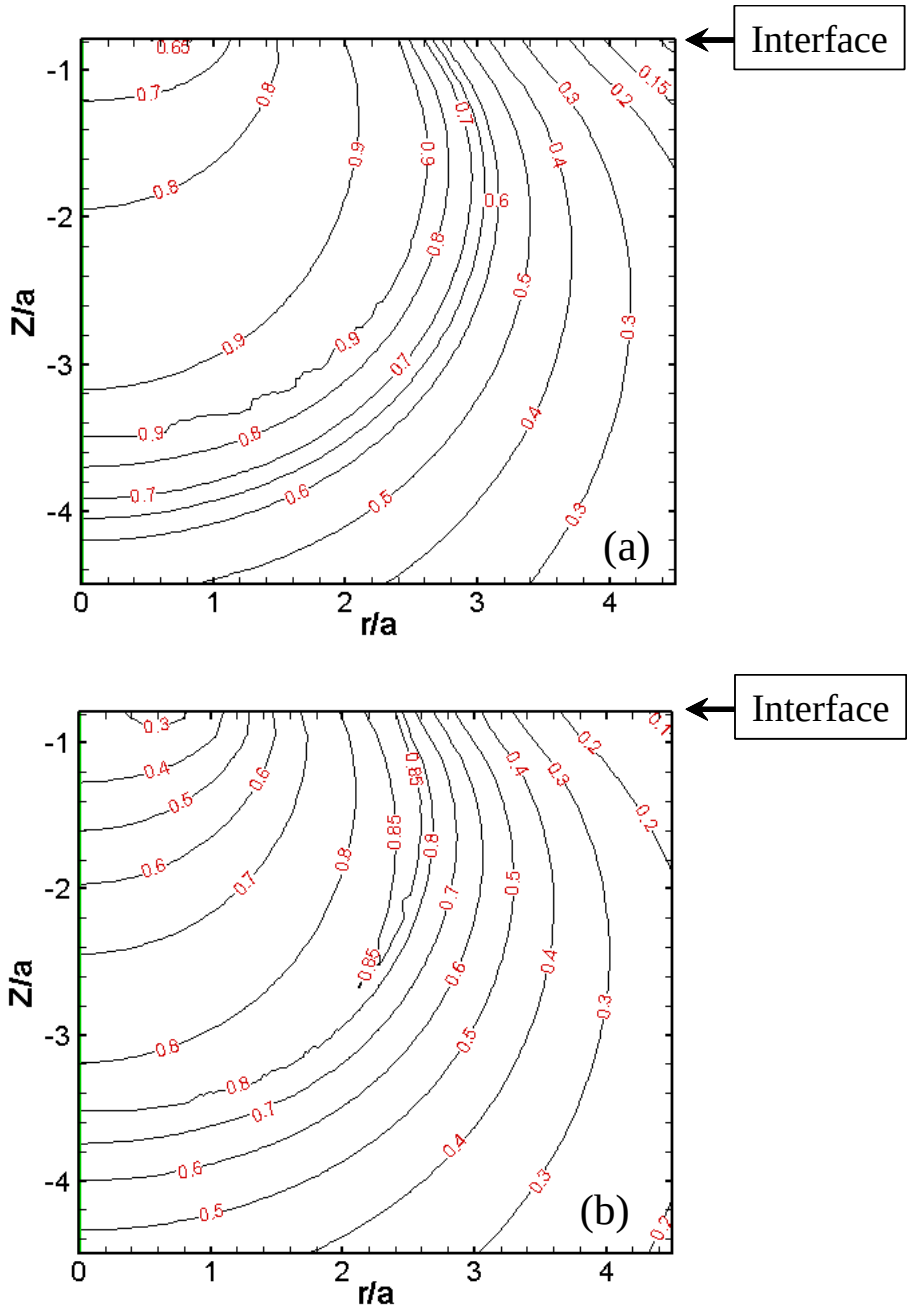

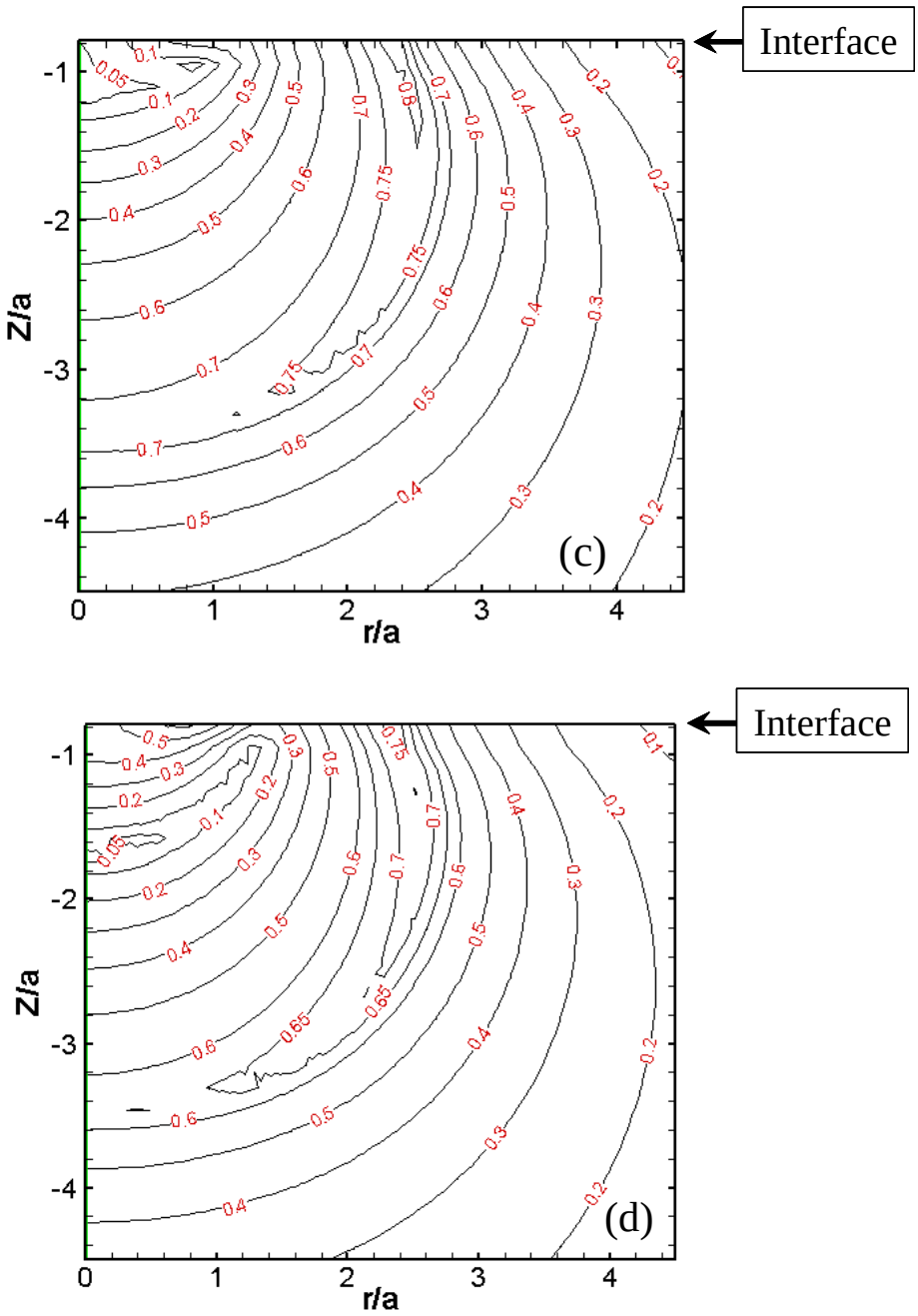

The ends of the contour line are now on the axis of symmetry and at the interface. As can be seen in figure 8-f, the region delimited by the ellipse is the final yielded zone upon unloading. The correlations between this deformation process and the resulting residual profile are under investigation.

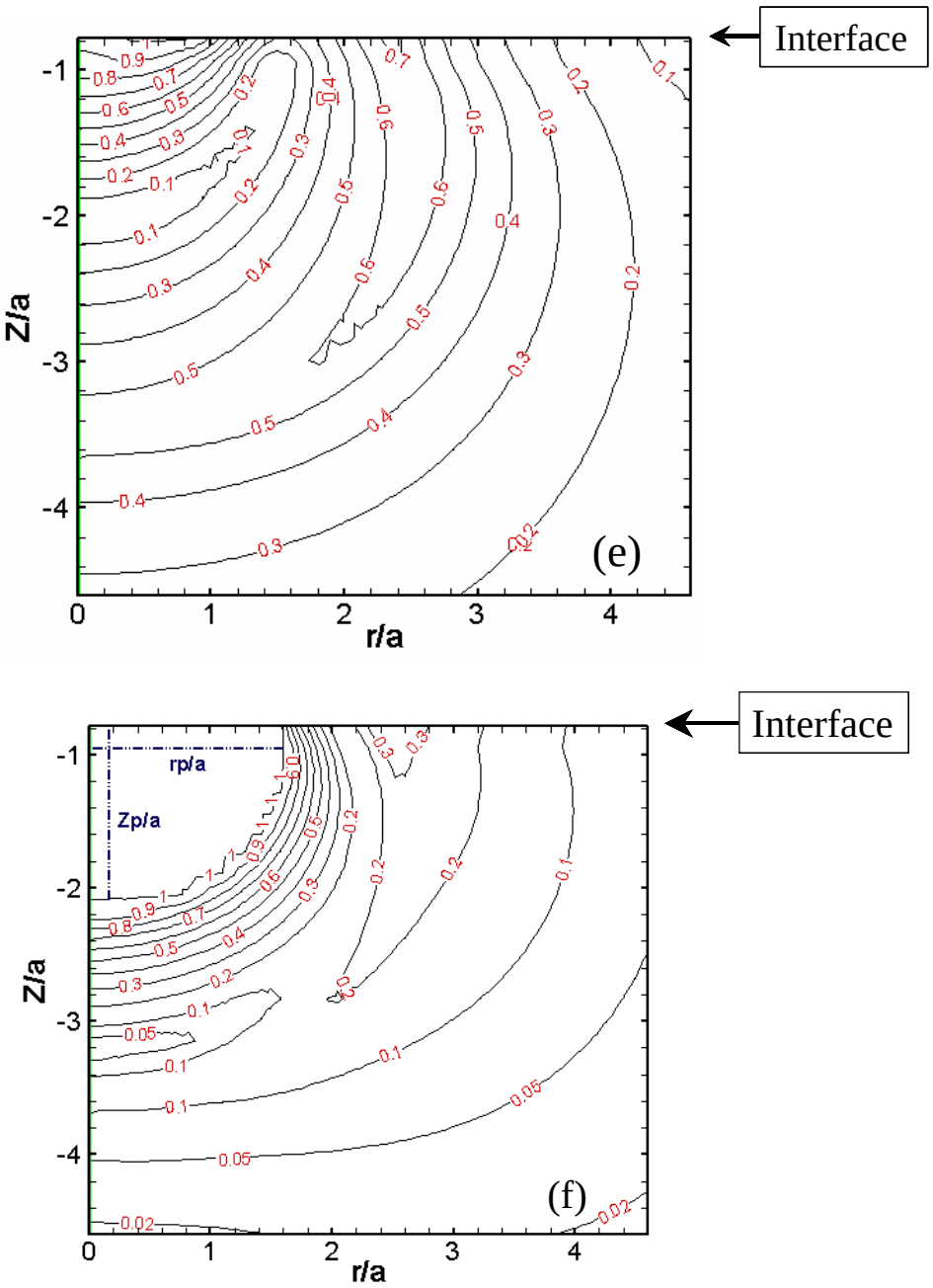

Figure 8. Film/substrate system (R = 50 µm, E^f/E^S = 2, t^f = 3 µm); Contour plot of the normalised von Mises stress after a) 10% unloading, b) 20% unloading, c) 30% unloading, d) 40% unloading, e) 50% unloading and f) 100% unloading; *a* is the contact radius at maximum load F/F* =14,3 (interface: *Z/a* = - 0.79).

c) Residual Axial Stress Perpendicular to the Loaded Surface

Well understood, if one is to get an idea about the nature of the stress fields in this volume, the von Mises stress is insufficient. In figure 9 we present the axial stress component of the strained volume normal to the free surface.

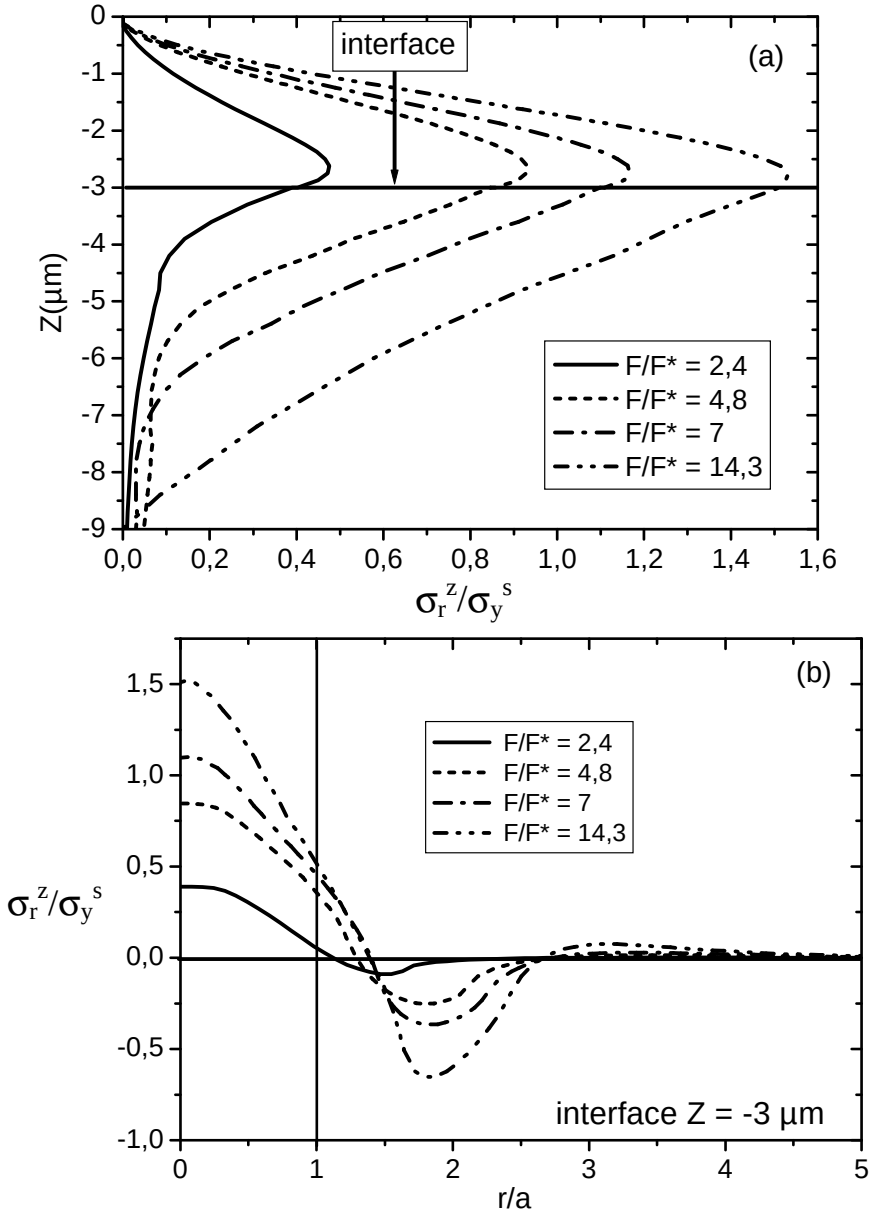

Figure 9. Film/substrate system; Residual axial stress at the interface (after complete unloading) for different maximum levels loads applied F/F* less than 300 mN. F* is the load of first substrate yielding; *a* is the radius of contact corresponding to the level of maximum load applied and σ_y^s the substrate yield stress. a) in the axial direction (*Z*) and b) in the radial direction (*r*).

In figure 9a we plot in abscissa the normalised residual axial stress component σ_r^z/σ_y^s perpendicular to the loaded surface (as above with F/F* as parameter) along the axis of symmetry Z. For all cases considered, there is a tensile stress maximum in the coating slightly above the interface whose intensity increases with increasing level, F/F*. The variation of this axial stress component with the distance *r/a* from the axis of symmetry is shown in figure 9b. Clearly, the tensile stress region is situated in the entire contact zone surrounded by a compressive strain in the volume below the annular surface area well beyond the edge of the contact area. These specific results confirm the conclusion induced above from the difference in residual deformation between the free surface and the interface (cf. figure 5). They are in perfect agreement with experimental findings of brittle interfacial delamination when indenting ill adhered coatings. Also, from acoustic emission monitoring during depth sensing indentation of such coatings there is evidence of delamination triggered during the unloading part of the indentation plot when the tensile stress component builds up (cf. von Stebut et *al*, 1999).

CONCLUSION

For loads applied via a 50μm spherically tipped indenter and the specific mechanical parameters considered surface profiles generated for the stress-applied as well as for the entirely unloaded state show that lateral pile-up will occur on unloading only.

In the contact zone residual depth profiles at the free surface are attenuated compared to those at the interface, which is indicative of tensile type stresses along the normal to the interface.

For the adopted configuration, the onset of plastic flow occurs in the substrate right below the interface. The plastic volume generated in the substrate consecutively with increasing load first spreads more quickly in the lateral (radial) than in the vertical (axial) direction. For higher loads this tendency is inverted and the maximum “width” of the plastic zone shifts downwards into the substrate volume.

In the presence of plastic yielding within the substrate, the apparent contact radius as assessed numerically from a plot of the residual profile is considerably higher than that at maximum contact load. The former, when measured from the pile-up apex, can be compared with that based on the experimentally observable diameter of the residual plastic indent.

On unloading, entirely elastic recovery of the indented specimen is confirmed numerically for at least the first 25% of the unloading plot. Increasing build-up of tensile components follows between 50% and 100% unloading in the volume below the contact area confirming qualitative indications from the comparison of the profiles at the free surface and the interface.

In the present approach the indenter tip radius adopted is considered to be close to realistic asperity radii in contact problems. In metrology, if coating-specific mechanical parameters are to be assessed, the tip geometry must be downscaled in order to achieve critical stress conditions localised in the coating.

REFERENCES

Balas J, Sladek J, Sladek V (1989) Stress analysis by boundary element methods. *Amsterdam, Elsevier Science Publishers.*

Bhushan B (1999) Principles and Applications of Tribology. *John Wiley and Sons.*

Bolshakov A, Pharr GM (1998) Influence of pile-up on the measurement of mechanical properties by load and depth sensing indentation techniques, *Journal of Materials Research*, vol.13, N°4, pp.1049-1058.

Bonnet M, Mukherjee S (1996) Implicit BEM formulations for usual and sensitivity problems in elasto-plasticity using consistent tangent operator concept. *International Journal of solids and structures*, vol.30, n 30, pp.4461-4480.

Christensen PW, Klarbring A, Pang JS, Strömberg N (1998) Formulation and comparison of algorithms for frictional contact problems. *International Journal for numerical methods in engineering* vol.42, n°1, pp.145-173.

Edlinger ML, Gratacos P, Montmitonnet P, Felder E (1993) Finite element analysis of elastoplastic indentation with a deformable indenter. *European Journal of Mechanics. A. Solids*, vol.12, n°5, pp.679-698.

Field JS, Swain MV (1993) A simple predictive model for spherical indentation. *Journal of Materials Research*, vol.8, n°2, pp.297-306.

Fischer-Cripps AC (2002) Nanoindentation, *Mechanical Engineering Series, Springer-Verlag, New York*, pp.197.

Garrido MA, Rodriguez J (2005) Pile-up effect on nanoindentation tests with spherical-conical tips, *Scripta Materialia*, vol.52, n°7, pp.593-598.

Hardy C, Baronet CN, Tordion GV (1971) The Elasto-plastic Indentation of half-space by a rigid sphere, *International Journal for numerical methods in engineering*, vol.3, pp.451-462.

Henry DP, Banerjee PK (1988) A variable stiffness type boundary element formulation for axisymmetric elastoplastic media. *International Journal for numerical methods in engineering*, vol.26, n°5, pp.1005-1027.

Johnson KL (1985) Contact Mechanics. *Cambridge University Press, Cambridge UK.* pp.171.

Kouitat Njiwa R, von Stebut J (2003) Boundary element numerical analysis of elastic indentation of a sphere into a bi-layer material. *International Journal of Mechanical Sciences*, vol.45, pp.317-324.

Kuhn G, Partheymüller P, Köhler O (1998) Regularization and evaluation of Singular Domain Integrals in Boundary Element methods; Singular Integral in BEM Evalued by V Sladek and J Sladek. *Computationnal Mechanics Publication*, pp.223-261.

Loubet JL, Georges JM, Meille G (1986) Vickers indentation curves of elastoplastic materials. Microindentation Techniques in *Materials Science and Engineering, ASTM STP 889*, PJ Blau and BR Lawn Eds, *American Society for Testing and Materials, Philadelphia*, pp.72-89.

Mata M, Anglada M, Alcala J (2002) Contact deformation regimes around sharp indentations and the concept of the chararcteristic strain. *Journal of Materials Research*, vol.17, n°5, pp.964-976.

McElhaney KW, Vlassak JJ, Nix WD, (1998) Determination of indenter tip geometry and indentation contact area for depth sensing indentation experiments, *Journal of Materials Research*, vol.13, n°5, pp.1300-1306.

Mesavoric SD, Fleck NA (1999) Spherical indentation of elastic-plastic solids. *Proceedings of the Royal Society London A* 445, pp.2707-2728.

Oliver WC, Pharr GM (1992) An improved technique for determining hardness and elastic modulus using load and displacement sensing indentation experiments. *Journal of Materials Research*, vol.7, n°6, pp.1564-1583.

Saha R, Nix WD (2002) Effects of the substrate on the determination of thin film mechanical properties by nanoindentation. *Acta Materiala*, vol.50, pp.23-38.

Saha R, Nix WD (2001) Soft films on hard substrates – Nanoindentation of tungsten films on sapphire substrates. *Materials Science and Engineering*, A 319-321, pp.898-901.

Stempflé Ph, von Stebut J (2006) Nano-mechanical behaviour of the 3rd body generated in dry friction–Feedback effect of the 3rd body and influence of the surrounding environment on tribology of graphite. *Wear* 260, pp.601-614.

Taljat B, Pharr GM (2004) Development of pile-up during spherical indentation of elastic-plastic solids. *International Journal of solids and structures*, vol.41, n°14, pp.3891-3904.

von Stebut J, Lapostolle F, Bucsa M, Vallen H (1999) Acoustic emission monitoring of single cracking events and associated damage mechanism analysis in indentation and scratch testing. *Surface and coatings technology* vol.116-119, pp.160-171.